Development of a thiol-ene based screening platform for enzyme immobilization demonstrated using horseradish peroxidase

Hoffmann, Christian; Pinelo, Manuel; Woodley, John; Daugaard, Anders Egede

Published in:
Biotechnology Progress

Link to article, DOI:
10.1002/btpr.2526

Publication date:
2017

Document Version
Peer reviewed version

Biotechnology Progress
DOI 10.1002/btpr.2526

Development of a thiol-ene based screening platform for enzyme immobilization demonstrated using horseradish peroxidase

*Christian Hoffmann, Manuel Pinelo, John M. Woodley, Anders E. Daugaard**

C. Hoffmann, Assoc. Prof. A. E. Daugaard

Danish Polymer Centre, Department of Chemical and Biochemical Engineering, Technical University of Denmark, Søltofts Plads Building 229, 2800 Kgs. Lyngby, Denmark

*Corresponding author: adt@kt.dtu.dk

Assoc. Prof. M. Pinelo

Center for BioProcess Engineering, Department of Chemical and Biochemical Engineering, Technical University of Denmark, Søltofts Plads Building 229, 2800 Kgs. Lyngby, Denmark

Prof. J. M. Woodley

Process and Systems Engineering Center (PROSYS), Department of Chemical and Biochemical Engineering, Technical University of Denmark, Søltofts Plads Building 229, 2800 Kgs. Lyngby, Denmark

Keywords: thiol-ene chemistry, surface functionalization, enzyme immobilization, enzyme-surface interaction

doi: 10.1002/btpr.2526

Received: Apr 25, 2017; Revised: Jul 07, 2017; Accepted: Jul 10, 2017

Abstract

Efficient immobilization of enzymes on support surfaces requires an exact match between the surface chemistry and the specific enzyme. A successful match would normally be identified through time consuming screening of conventional resins in multiple experiments testing individual immobilization strategies. In this study we present a versatile strategy that largely expands the number of possible surface functionalities for enzyme immobilization in a single, generic platform. The combination of many individual surface chemistries and thus immobilization methods in one modular system permits faster and more efficient screening, which we believe will result in a higher chance of discovery of optimal surface/enzyme interactions.

The proposed system consists of a thiol-functional microplate prepared through fast photochemical curing of an off-stoichiometric thiol-ene (OSTE) mixture. Surface functionalization by thiol-ene chemistry (TEC) resulted in the formation of a functional monolayer in each well, whereas, polymer surface grafts were introduced through surface chain transfer free radical polymerization (SCT-FRP). Enzyme immobilization on the modified surfaces was evaluated by using a rhodamine labeled horseradish peroxidase (Rho-HRP) as a model enzyme, and the amount of immobilized enzyme was qualitatively assessed by fluorescence intensity (FI) measurements. Subsequently, Rho-HRP activity was measured directly on the surface. The broad range of utilized surface chemistries permits direct correlation of enzymatic activity to the surface functionality and improves the determination of promising enzyme-surface candidates. The results underline the high potential of this system as a screening platform for synergistic immobilization of enzymes onto thiol-ene polymer surfaces.

1. Introduction

Immobilized enzymes are widely used as biosensors, in drug delivery, as well as in dairy and food processes for the production of pharmaceuticals and cosmetics.[1,2] Their high substrate specificity, selectivity, and efficiency at mild reaction conditions, such as ambient temperature, physiological pH and atmospheric pressure make them interesting alternatives to conventional catalysts. However, as functional biocatalysts, enzymes frequently demonstrate limited operational stability. Immobilization of enzymes has generally been demonstrated to have a stabilizing effect due to stronger confinement in enzyme rigidity, which leads to improved pH, organic solvent and thermal stability.[3–5] However, increased stability and even improved selectivity or activity can only be achieved, when a favorable environment for the enzyme is obtained. Further advantages are the improved recovery and purification from reaction media and potential recirculation of immobilized biocatalysts in the process.[6] Depending on the application and the particular enzyme of interest, many strategies are available for immobilization with, or without, a support matrix.[7,8] Cross-linking enzymes by either physical or covalent interactions, leads to the formation of enzyme aggregates, which can directly be used.[9] Entrapment or binding to a support matrix requires the use of a solid carrier material.[10] However, a general concern of most of these procedures is the potential reduction in biocatalytic activity upon immobilization due to a combination of various individual factors, such as changes in conformation and accessibility to the active site.[11] These factors are greatly influenced when confining structural freedom or even changing their structural conformation upon immobilization.[12] In some specific cases, strong attachment of enzymes to a surface, for instance by multibond attachment, might also have a beneficial effect for the activity in addition to improvements in stability due to conformational restrictions of the enzyme.[13]

For the attachment of enzymes to the surface of solid supports various factors for stabilization and destabilization have been identified and reviewed by Talbert and Goddard.[14] In order to

prevent deactivation, the properties of the surface (hydrophilicity, hydrophobicity, charge, surface topology, and functionality) have to match structural and compositional characteristics of a particular enzyme and provide a favorable local environment for immobilized enzyme.[15] Each enzyme or protein has a unique structure and generalizations about stabilization effects on specific surfaces are therefore not universal applicable. For this reason different approaches have been investigated in order to achieve surface modifications, which can lead to improved biocatalytic activity of immobilized enzymes. Surface functionalizations with charged[16,17], hydrophilic[18] or hydrophobic[19] moieties as well as functional groups, to which enzymes can bind covalently[20], have been investigated. Direct attachment to the surface via covalent binding leads to structurally confined and rigid immobilized enzymes with strong interactions between the surface and the enzyme.[14] Polymers grafted to or from a surface[21–23] as well as surface bound tethers[24,25] can act as spacers between surface and enzyme, which offers higher mobility of the enzyme. This may either result in an improved enzyme activity, or this may negatively impact the stability due to higher mobility and reduced rigidity. Consequently, the final result on activity and stability will be a balance between several effects, which should be identified for each specific enzyme.

Different materials like glass, metals or polymers can serve as a solid support for enzyme immobilization. The easy processibility of polymers, adjustable mechanical properties, conductivity, and ease of post-functionalization make polymers an extensively used support material.[26] Recently, the development of stoichiometric thiol-ene (STE) and furthermore off-stoichiometric thiol-ene (OSTE) polymer thermosets with tunable mechanical properties was reported.[27–30] OSTE materials show high compatibility with many solvents, are thermally stable and can directly be surface functionalized after preparation. Here, thiol and alkene containing monomers undergo cross-linking by thiol-ene chemistry (TEC) under radical conditions. TEC is an efficient method providing high yields under relatively mild reaction conditions.[31] This highly modular system has allowed STE and OSTE materials to be applied

for fabrication of microfluidics,[32,33] particles[34], hydrogels[35] or high internal phase emulsions (HIPE).[36] Variations in stoichiometry between the reagents lead to either unreacted thiol or alkene groups, which are present in the bulk OSTE material as well as on the surface. This excess of functional groups can be used further for surface modification via TEC.[37–40] Hence, surface hydrophilization, hydrophobization, as well as introduction of biological moieties has been reported.[41–43] Post preparation modification of the materials has even been shown to be possible by incorporation of glycidyl methacrylate into a photocurable TE material, which resulted in unreacted epoxide groups after curing. These residual functionalities were used for covalent immobilization of α-amylase for the preparation of a biocatalytic surface.[44]

However, due to the vast amount of existing enzyme support resins, the selection of a suitable candidate for specific enzymes is very difficult, as a beneficial match surface-enzyme cannot be generally predicted by just considering the chemistry of the support surface and its potential interaction with the enzyme. For instance, these interactions can be of hydrophilic or hydrophobic nature as well as formed hydrogen bonds, which show a different influence on different enzymes and thus, impact their biocatalytic performance. Therefore, the objective of this study was to develop a single, versatile platform that allows broader screening of different surface chemistries for enzyme immobilization. For this purpose the high modularity in preparation of TE materials and their possibility for facile surface modification was exploited to illustrate their potential as support for the immobilization of enzymes. An STE/OSTE microplate was fabricated, which enabled versatile surface functionalization via photochemical TEC or in a new approach through surface chain transfer free radical polymerization (SCT-FRP). Initial activity measurements of immobilized horseradish peroxidase as a model enzyme on those surfaces were conducted, which were used for evaluation of beneficial surface chemistries as enzyme support. Such a microplate permits screening of synergistic interactions between enzymes and surfaces in a time-saving,

systematic approach, which should enable facile identification of efficient immobilization systems.

2. Materials and Methods

Materials

Pentaerythritol tetrakis(3-mercaptopropionate) (PETMP, >95%), 1,3,5-Triallyl-1,3,5-triazine-2,4,6(1H,3H,5H)-trione (TATATO, 98%), allyl pentafluorobenzene (APFB, >99%), allyltrifluoroacetate (ATFA , 98%), allyl alcohol (AA, 99%), allyl malonic acid (AMA, ≥98%), 1-vinyl imidazole (Vim, ≥99%), allylamine hydrochloride (Aam, 98%), [2-(Methacryloyloxy)ethyl]dimethyl-(3-sulfopropyl)ammonium hydroxide (97%) as a sulfobetaine methacrylate (SBMA), 2,2-dimethoxy-2-phenylacetophenone (DMPA, 99%), allyl glycidyl ether (AGE, >99%), horseradish peroxidase (HRP, lyophilized powder, 50-150 U mg^{-1}), 2,2′-Azino-bis(3-ethylbenzothiazoline-6-sulfonic acid) diammonium salt (ABTS, ≥98%) and hydrogen peroxide (H_2O_2, 3%) were obtained from Sigma Aldrich and used without further purification.

Methoxy poly(ethylene glycol) monomethacrylate (MPEGMA, M_n 500), glycidyl methacrylate (GMA, 97%) and 2,2,3,3,4,4,5,5 octafluoropentyl acrylate (OFPA, 97%) were purchased from Sigma Aldrich and passed through a short plug flow column containing aluminum oxide (Sigma-Aldrich, activated, basic, Brockmann I, standard grade) prior to use. Ethanol was obtained from VWR Chemical. Lucirin TPO-L (ethyl-2, 4, 6-tri-methylbenzoylphenyl phosphinate) was obtained from IGM Resins. Sylgard 184 – poly(dimethylsiloxane) (PDMS) elastomer kit was purchased from Dow Corning.

Characterization.

Fourier transform infrared (FT-IR) spectroscopy was carried out using a Nicolet iS50 FT-IR fitted with a diamond crystal attenuated total reflection accessory (ATR), which operated at a resolution of 4 cm^{-1} and 32 scans per measurement and was used to identify chemical

modifications made by surface functionalization. XPS experiments were conducted on a Thermo Fisher Scientific K-Alpha (East Grinstead, UK). Large area surface analysis used a 400 μm spot of monochromatized aluminum Kα radiation, following which survey (pass energy 200 eV) and high-resolution (pass energy 50 eV) spectra for relevant elements were acquired. Data analyses of the obtained XPS spectra were performed using the Avantage software package as provided by the manufacturer. Average values and standard deviations were conducted for each surface in technical replicates of three (n=3). Static water contact angles (WCAs) of the virgin and functionalized OSTE surfaces were determined by using a Dataphysics Contact Angle System OCA20. Each surface was tested via the static sessile drop method at 23°C, the average value and standard deviations were determined from three technical replicates (n=3).

The immobilization yield of rhodamine labeled HRP in the wells was determined using a POLARstar® Omega from BMG Labtech equipped with a fluorescence probe (gain of 1000 as a general setting of the instrument) at 25 °C. This value was subtracted by the fluorescence intensity result measured prior enzyme immobilization. The enzyme activity of immobilized Rho-HRP was determined by absorbance measurements (at 414 nm) using a POLARstar® Omega from BMG Labtech equipped with a UV-VIS probe (20 scans per measurement) at 25 °C. For each surface, immobilization of Rho-HRP including FI and enzyme activity measurements, were performed in experimental replicates of three (n=3), from which the average values and standard deviations were calculated.

Preparation of OSTE microtiter plate.

In a stoichiometric ratio between thiol and ene groups, PETMP (24.44 g, 0.050 mol, 0.20 mol *thiol*), TATATO (16.64 g, 0.067 mol, 0.20 mol *ene*) and TPO-L (11.1 mg, 0.03 wt%) were mixed with a dual asymmetric centrifuge Speed-Mixer, High Wycombe, UK, DAC 150 FVZ-K at 2500 to 3500 r.p.m. for 2 min screened from ambient light. A previously prepared PDMS

mold with the negative imprint of the top part of the microtiter plate was filled with this mixture, which was subsequently cured under UV light (λ= 365 nm, 2.9 mW cm^{-2}) for 3 min. Then, PETMP (22.06 g, 0.045 mol, 0.18 mol *thiol*), TATATO (7.91 g, 0.032 mol, 0.095 mol *ene*) and TPO-L (8.1 mg, 0.03 wt%) were mixed in a Speed-mixer and a second PDMS mold for the bottom component was filled with this mixture. This mixture was left under sunlight for 7 min and then the previously top component was attached from the top. This assembly was again cured under UV light (λ= 365 nm, 2.9 mW cm^{-2}) for 3 min resulting in the final microwell plate. A schematic drawing with measures of the top and bottom component of the microwell plate separately is shown in Figure S1.

IR (cm^{-1}): 2961 (C-H), 2571 (S-H), 1731 (C=O), 1678 ($C=C_{alkene}$), 1459 ($O-CH_{2\ ester}$), 1351, 1141 ($C-O-C_{stretch\ vibr}$), 1021 (C-O-C), 764($C-O-C_{deformation}$), 528.

Surface functionalization via TEC with allyl pentafluorobenzene (OSTE-APFB).

In a general functionalization procedure, an ethanolic solution (10 mL) containing APFB (0.460 mL, 3.0 mmol) and TPO-L (9.9 mg, 1 mol%) was prepared screened from ambient light. 300 µL of this solution was added to a single well and subsequently irradiated with UV light (λ= 365 nm, 2.9 mW cm^{-2}) for 5 min. Subsequently, the well was thoroughly rinsed with Ethanol and finally blow dried with air. Typically, five replicates of each modification were prepared.

IR (cm^{-1}): 2959 (C-H), 2567 (S-H), 1730 (C=O), 1678 ($C=C_{alkene}$), 1459 ($O-CH_{2\ ester}$), 1352, 1140 ($C-O-C_{stretch\ vibr}$), 1022 (C-O-C), 764 ($C-O-C_{deformation}$), 528.

Preparation of OSTE-ATFA.

OSTE-ATFA was prepared in accordance with the general procedure, using 300 µL of an ethanolic solution (10 mL) of allyltrifluoroacetate (ATFA, 0.27 mL, 2.1 mmol) and TPO-L (9.0 mg, 0.7 mol%) as reagents.

IR (cm^{-1}): 2961 (C-H), 2571 (S-H), 1731 (C=O), 1678 ($C=C_{alkene}$), 1459 ($O-CH_{2\ ester}$), 1353, 1141 ($C-O-C_{stretch\ vibr}$), 1021 (C-O-C), 764 ($C-O-C_{deformation}$), 528.

Preparation of OSTE-OFPA. OSTE-OPFA was prepared in accordance with the general procedure, using 300 µL an ethanolic solution (10 mL) of 2,2,3,3,4,4,5,5 octafluoropentyl acrylate (OFPA, 0.58 mL, 3.0 mmol) and TPO-L (9.3 mg, 0.97 mol%) as reagent.

IR (cm^{-1}): 2961 (C-H), 2570 (S-H), 1730 (C=O), 1678 ($C=C_{alkene}$), 1459 ($O-CH_{2\ ester}$), 1353, 1141 ($C-O-C_{stretch\ vibr}$), 1021 (C-O-C), 764 ($C-O-C_{deformation}$), 528.

Preparation of OSTE-AA. OSTE-AA was prepared in accordance with the general procedure, using 300 µL of an ethanolic solution (10 mL) of allyl alcohol (AA, 0.20 mL, 3.0 mmol) and TPO-L (10.5 mg, 1.1 mol%) as reagent.

IR (cm^{-1}): 2961 (C-H), 2570 (S-H), 1731 (C=O), 1678 ($C=C_{alkene}$), 1459 ($O-CH_{2\ ester}$), 1353, 1141 ($C-O-C_{stretch\ vibr}$), 1020 (C-O-C), 764 ($C-O-C_{deformation}$), 528.

Preparation of OSTE-AMA. OSTE-AMA was prepared in accordance with the general procedure, using 300 µL of an ethanolic solution (10 mL) of allyl malonic acid (AMA, 0.433 g, 3.0 mmol) and TPO-L (10.4 mg, 1.1 mol%) as reagent.

IR (cm^{-1}): 2961 (C-H), 2571 (S-H), 1731 (C=O), 1678 ($C=C_{alkene}$), 1459 ($O-CH_{2\ ester}$), 1353, 1141 ($C-O-C_{stretch\ vibr}$), 1021 (C-O-C), 764 ($C-O-C_{deformation}$), 528.

Preparation of OSTE-Vim. OSTE-Vim was prepared in accordance with the general procedure, using 300 µL of an ethanolic solution (10 mL) of 1-vinyl imidazole (Vim, 0.30 mL, 3.0 mmol) and TPO-L (9.2 mg, 1.0 mol%) as reagent.

IR (cm^{-1}): 3136 (N-H), 2961 (C-H), 2571 (S-H), 1730 (C=O), 1677 ($C=C_{alkene}$), 1459 ($O-CH_{2\ ester}$), 1352, 1139 ($C-O-C_{stretch\ vibr}$), 1024 (C-O-C), 763 ($C-O-C_{deformation}$), 528.

Preparation of OSTE-AGE. OSTE-AGE was prepared in accordance with the general procedure, using 300 µL of an ethanolic solution (10 mL) of allyl glycidyl ether (AGE, 0.36 mL, 3.0 mmol) and TPO-L (9.0 mg, 0.97 mol%) as reagent.

IR (cm^{-1}): 2961 (C-H), 2567 (S-H), 1730 (C=O), 1678 ($C=C_{alkene}$), 1459 ($O-CH_{2\ ester}$), 1353, 1140 ($C-O-C_{stretch\ vibr}$), 1021 (C-O-C), 764 ($C-O-C_{deformation}$), 527.

Preparation of OSTE-Aam hc. OSTE-Aam hc was prepared in accordance with the general procedure, using 300 µL of an ethanolic solution (10 mL) of allylamine hydrochloride (Aam hc, 0.281 g, 3.0 mmol) and TPO-L (10.1 mg, 1.1 mol%) as reagent.

IR (cm^{-1}): 2962 (C-H), 2571 (S-H), 1731 (C=O), 1678 ($C=C_{alkene}$), 1459 ($O-CH_{2\ ester}$), 1353, 1141 ($C-O-C_{stretch\ vibr}$), 1020 (C-O-C), 764 ($C-O-C_{deformation}$), 528.

Surface functionalization via surface chain transfer free radical polymerization (SCT FRP) with poly(ethylene glycol) methylether methacrylate (OSTE-g-pMPEGMA).

In a general procedure Methoxy poly(ethylene glycol) monomethacrylate (MPEGMA, 0.92 mL, 2.0 mmol) and 2,2-dimethoxy-2-phenylacetophenone (DMPA, 2.6 mg, 0.50 mol%) were dissolved in ethanol (1.85 mL) screened from ambient light. 300 µL of this solution was added to a single well and subsequently irradiated with UV light (λ= 365 nm, 2.9 mW cm^{-2}) for 30 min. Subsequently, the well was thoroughly rinsed with Ethanol and finally blow dried with air. Typically, five wells in the same well plates were functionalized.

IR (cm^{-1}): 2871 (C-H), 1733 (C=O), 1684 ($C=C_{alkene}$), 1461 ($O-CH_{2\ ester}$), 1349, 1101 ($C-O-C_{stretch\ vibr}$), 1035 (C-O-C), 944, 852, 764 ($C-O-C_{deformation}$), 528.

Preparation of OSTE-g-pGMA. OSTE-g-pGMA was prepared in accordance with the general procedure, using 300 µL of a solution of glycidyl methacrylate (GMA, 0.453 mL, 3.3 mmol), DMPA (4.3 mg, 0.5 mol%) in ethanol (0.91 mL) as reagents.

IR (cm^{-1}): 2999 ($C-H_{epoxide}$), 2936 (C-H), 1724 (C=O), 1685 ($C=C_{alkene}$), 1449 ($O-CH_{2\ ester}$), 1129 ($C-O_{stretch\ vibr}$), 989 (C-O), 904 (epoxide ring vibr), 841 (C-C), 757 ($C-O-C_{deformation}$).

Preparation of OSTE-g-pSBMA. OSTE-g-pSBMA was prepared in accordance with the general procedure, using 300 µL of a solution of [2-(methacryloyloxy)ethyl]dimethyl-(3-sulfopropyl)ammonium hydroxide (SBMA, 0.846 g, 3.0 mmol), DMPA (3.9 mg, 0.5 mol%) in ethanol (1.28 mL) as reagents.

IR (cm^{-1}): 3443 (N-H), 2964 (C-H), 1726 (C=O), 1676 ($C=C_{alkene}$), 1459 ($O-CH_{2\ ester}$), 1143 ($C-O_{stretch\ vibr}$), 1035, 901, 762 ($C-O-C_{deformation}$), 603, 524.

Preparation of OSTE-g-pOFPA. OSTE-g-pOFPA was prepared in accordance with the general procedure, using 300 µL of a solution of 2,2,3,3,4,4,5,5 octafluoropentyl acrylate (OFPA, 1.25 mL, 3.0 mmol), DMPA (3.1 mg, 0.4 mol%) in ethanol (0.93 mL) as reagents.

IR (cm^{-1}): 2968 (C-H), 1737 (C=O), 1684 ($C=C_{alkene}$), 1464 ($O-CH_{2\ ester}$), 1163 (C-F), 1124 ($C-O_{stretch\ vibr}$), 1044, 805, 765 ($C-O-C_{deformation}$), 539 (C-F).

Labelling of horseradish peroxidase.

Horseradish peroxidase (10.0 mg) was dissolved in sodium carbonate buffer (0.1M, pH 9.5, 1.0 mL) and 20 µL of sulforhodamine B acid chloride in DMF (10 mg mL^{-1}) was added dropwise under mild vortex mixing was added. This solution was incubated at 4 °C overnight and subsequently purified by dialysis for 3 days against PBS buffer. The purified solution was stored at 4 °C for further use.

Immobilization of horseradish peroxidase.

The previously labelled Rho-HRP solution (0.455 mL) was diluted with PBS buffer (pH 7.3, 1.0 mL), and 300 µL of this solution was added to each well. In order to prevent evaporation of liquid the plate was covered with a PDMS cover and incubated at 4 °C for 16 h. Then, the supernatant was removed and PBS buffer (300µL) was added to the well. The rinsing buffer was replaced 4 times while slowly shaking. The immobilization yield was determined via fluorescence intensity measurement of the surface.

Activity assay of bioactive surfaces.

A phosphate buffer solution (0.1M, pH5, 300 µL) containing 2,2′-azino-bis(3-ethylbenzothiazoline-6-sulfonic acid) diammonium salt (ABTS, 1.0 mM) and hydrogen peroxide (10 mM) was added into a well with immobilized Rho-HRP. In the presence of H_2O_2, ABTS (absorbance maximum at 340 nm) is oxidized by HRP to $ABTS^{\bullet+}$, which shifts the absorbance maximum to 412 nm (ε_{412}=3.6 x $10^4 M^{-1}$ cm^{-1}).[45]

The absorbance at 412 nm corresponding to the absorbance maximum of the oxidized product ($ABTS^{\bullet+}$) was measured, which corresponds directly to the concentration of the product. The measurements were conducted every 20 s over 10 min directly through the well including shaking (10s, 300 r.p.m.) between each measurement. The slope of the measurements was used as a measure for the activity of the immobilized Rho-HRP on the surface.

3. Results and Discussion

The preparation of STE/OSTE microplates was based on a 2-step curing process via photoinitiated TEC using pentaerythritol tetrakis(3-mercaptopropionate) (PETMP) and 1,3,5-triallyl-1,3,5-triazine-2,4,6(1H,3H,5H)-trione (TATATO) as shown in Figure 1A.

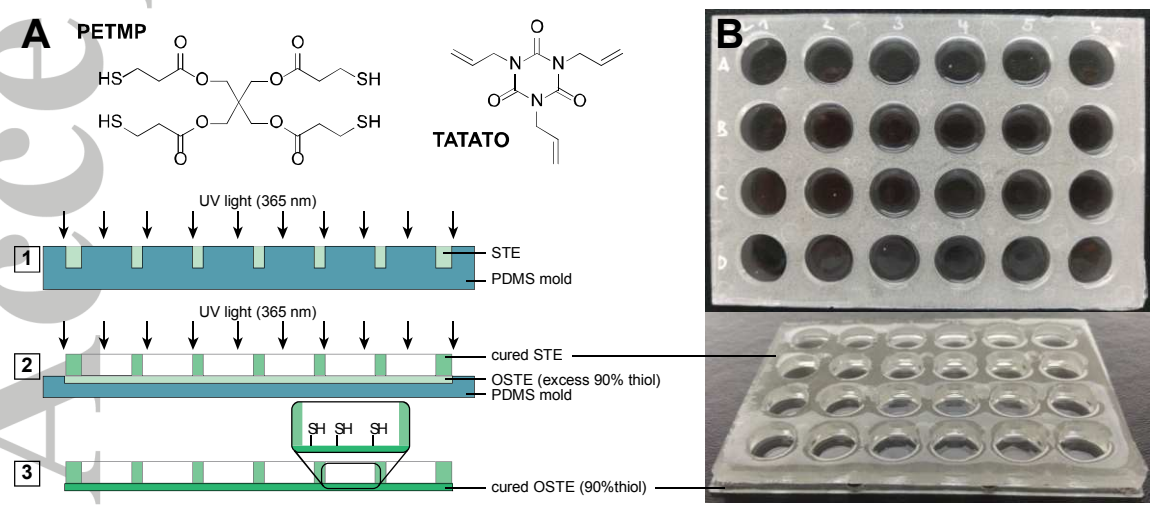

Figure 1 (A) schematic representation of the microplate preparation using a 2-step curing process, (1) curing by irradiation with UV light of the top part prepared from a stoichiometric thiol-ene (STE) mixture of PETMP and TATATO in a PDMS mold, (2) the prepared top part is placed on a OSTE mixture (excess 90% thiol) of PETMP and TATATO, where a second curing step by irradiation with UV light leads to the final microplate, (3) which contain excess thiol groups in the bottom and STE on the well walls, (B) Photographs of the final microwell plate.

In a first stage, the top part of the microplate in a STE mixture of PETMP and TATATO was photochemically cured in the presence of TPO-L in a poly(dimethylsiloxane) (PDMS) mold, as shown in Figure 1A-1. The mold consisted of the outer geometries of the microplate (127.7 x 85.6 mm^2), pillars with the size of the round wells (diameter 15.1 mm) and a depth of 5 mm. A second mold with a depth of 1.5 mm and the outer diameters of the microtiter plate was then applied for the second curing step. Here, an OSTE composition of PETMP, TATATO and TPO-L using a 90 % excess of thiol was applied for the well bottom. The previously prepared STE top part was then placed on top of the uncured OSTE mixture and both parts were cured together (see Figure 1A-2). This preparation process resulted in a fully sealed microplate consisting of 24 wells with a depth of 5 mm, shown in Figure 1A-3 and Figure 1B. Due to the used compositions, excess thiol groups remained on the bottom of each well. The side walls of the wells, based on a STE composition, did not contain any residual thiols, as determined using Ellman's reagent, which is commonly used for quantification of thiol groups either on surfaces or in solution (see Figure S2).[46] From these results it could be seen that Ellman's reagent, which was added to a STE surface, exhibit a very low absorbance compared to the OSTE with 90 % excess of thiols. Therefore, it was deduced that the number of thiols on the side walls was considered negligible and that modification of surface bound thiols occurred exclusively on the bottom surfaces. Furthermore, the transmittance of the OSTE

material was measured in order to validate the possible application in colorimetric assays. The material demonstrated a strong absorbance in the UV range from 220 to 340 nm, as shown in Figure S3. Between 340 and 410 nm, the transmittance increased up to 36 % (absorbance = 0.44) and at any wavelength above, the material was completely transparent (absorbance < 0.15). In general, the absorbance of the STE/OSTE microplate does not substantially differ from a commercial polystyrene microplate, as indicated in Figure S3. Therefore, the STE/OSTE plate is well suited for any application in which absorbance measurements of solutions or surface modifications are performed.

Excess thiol groups on the bottom surface originating from the OSTE mixture allow controlled surface functionalization via TEC and SCT-FRP. In this study, the surface modification using both methods has been attempted with a large range of monomers in order to introduce different types of functionalities as illustrated in Scheme 1.

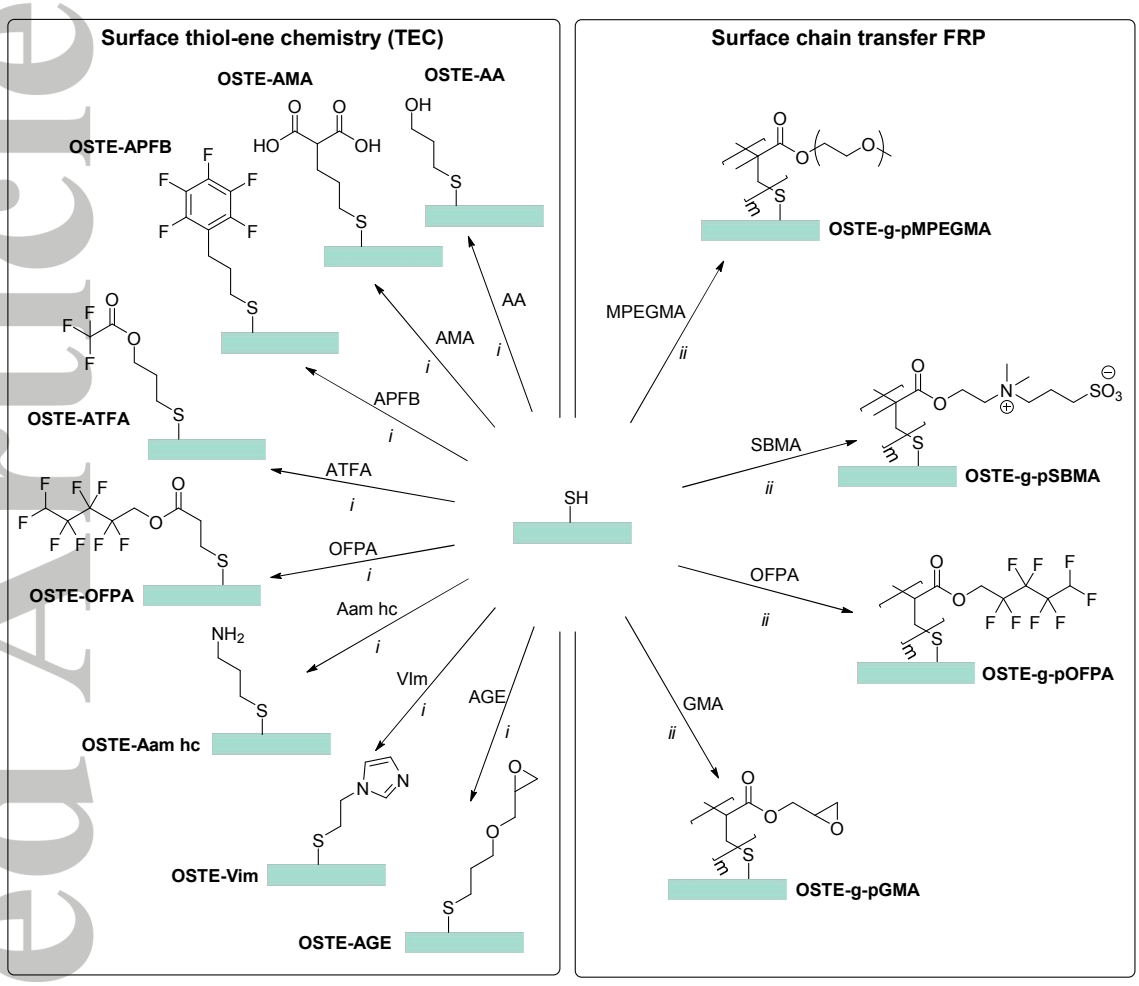

Scheme 1. Surface functionalization of thiols from OSTE microwell surfaces via two different routes; left: surface thiol-ene chemistry (TEC) with allyl alcohol (AA), allyl malonic acid (AMA), allyl pentafluorobenzene (APFB), allyl trifluoroacetate (ATFA), 2,2,3,3,4,4,5,5 octafluoropentyl acrylate (OFPA), allyl amine hydrochloride (Aam hc), 1-vinyl imidazole (Vim) and allyl glycidyl ether (AGE) at low concentration (0.3 M) leading to a functional monolayer on the surface; right: SCT-FRP with methoxy poly(ethylene glycol) methacrylate (MPEGMA), zwitterionic sulfobetaine methacrylate (SBMA, via [2-(methacryloyloxy)ethyl]dimethyl-(3-sulfopropyl)ammonium hydroxide), OFPA and glycidyl methacrylate (GMA) based monomers at high concentration (0.7 – 2.4 M), leading to a functional polymer grafted surface.

With the aim to develop a platform for enzyme immobilization, which enables screening of various surface functionalities and their impact on the activity of surface bound enzymes, a variety of functional monomers were utilized under TEC conditions. Based on different types of possible interactions and immobilization mechanisms various reactive moieties were selected. Hydroxyl functional groups (AA) were introduced as well as fluorine groups (APFB, ATFA and OFPA). pH responsive modifications, with either acidic groups (AMA) or basic functionalities, such as amine (Aam hc) and imidazole (Vim) were used as well. This range of introduced surface chemistries offered possible immobilization mechanisms including hydrophilic (with OSTE-AA, -AMA), hydrophobic (OSTE-APFB, -ATFA, -OFPA) and ionic interactions (OSTE-Vim and -AMA). Furthermore, epoxides were introduced (AGE) allowing bioconjugation through covalent enzymes binding with amine, thiol, imidazole or phenolic moieties from the enzyme.[6] The application of such a broad range of reagents demonstrates the great versatility of this process and can extensively be expanded, since TEC offers a vast range of surface chemistries by reaction of any allyl, vinyl or acrylic compound onto the screening platform. Photochemical surface TEC was performed with low monomer concentrations (0.3 M) in ethanol solutions in order to prevent polymerization reactions. The IR spectrum of the starting material (OSTE) contains typical alkane (C-H, 2968 cm^{-1}), carbonyl (C=O, 1729 cm^{-1}), alkene (C=C, 1683 cm^{-1}) and aliphatic ester (C-O-C, 1141 cm^{-1}) elements. Comparison with TEC grafted surfaces did not exhibit significant differences, as illustrated in Figure S4. This could be explained by a low surface coverage due to a TE addition on the surface. Small structural changes as a result of monolayer formation can generally not be detected by attenuated total reflectance (ATR) FT-IR due to the domination of the bulk material in the spectrum, caused by the penetration depth of the IR signal. However, by using X-ray photoelectron spectroscopy (XPS) in combination with static water contact angle (WCA) measurements, the individual modifications were confirmed, as shown in Table 1 for the virgin (OSTE) and TEC modified surfaces.

Table 1. XPS data and static water contact angles (WCA) of virgin and functionalized OSTE surfaces via TEC with a variety of ene compounds

	C1s [atom%]	O1s [atom%]	N1s [atom%]	S2p [atom%]	F1s [atom%]	WCA [°]
OSTE	61.1±0.6 (60.6)	23.3±0.2 (24.9)	4.5±0.3 (4.1)	11.1±0.3 (10.4)		67.0±1.2
OSTE-APFB	58.8±2.8	27.2±2.0	2.7±0.0	9.9±0.5	1.4±0.3	62.4±2.1
OSTE-ATFA	55.3±0.0	28.6±0.1	5.2±0.2	8.1±0.2	2.8±0.1	41.1±2.4
OSTE-OPFA	53.4±0.4	26.9±0.1	4.5±0.3	8.1±0.0	7.1±0.6	77.7±4.1
OSTE-AA	60.4±0.2	27.6±0.7	4.5±0.5	7.6±0.4		35.0±1.5
OSTE-AMA	61.3±0.1	27.8±0.1	4.2±0.0	6.7±0.1		25.1±3.6
OSTE-Vim	63.3±1.5	22.6±0.8	7.3±0.2	6.8±0.5		38.5±3.6
OSTE-AGE	58.7±0.6	28.7±0.3	4.2±0.3	8.4±0.2		55.9±3.7
OSTE-Aam hc	59.3±0.2	26.5±0.1	5.5±0.1	8.7±0.1		55.4±4.7

In parenthesis, theoretical atom composition of the virgin surface (OSTE), results are based on three replicated measurements on the same surface (n=3)

The atom composition of the unreacted OSTE surface estimated by XPS was in agreement with the theoretical values and therefore used for further comparisons with modified surfaces. Surface functionalization with fluorinated reagents such as APFB, ATFA and OFPA was confirmed by the presence of fluorine atoms (F1s) in the XPS spectra, which was not detected on the native OSTE surface. APFB modified OSTE exhibited with 1.4 atom% the lowest fluorine content, which suggested a low grafting efficiency. This could be improved by reaction with ATFA and OFPA (2.8 and 7.1 atom%). In contrast to the allylic reagents, OFPA being an acrylic monomer is prone to undergo polymerization under radical conditions. Here, the overall atom composition of OFPA modified surfaces under TEC conditions, showed

additional to the increase in fluorine content a slight reduction in carbon, sulfur and nitrogen. This confirmed that under the applied low concentration TEC conditions, even for an acrylic monomer, like OFPA, the addition reaction dominated, leading to the formation of a monolayer (polymerization could then be suppressed). The atom composition after surface TEC with AMA, AA and AGE did not differ significantly from the reference OSTE surface. This could be attributed to similar theoretical atom composition of these reagents and the OSTE base material. In contrast, surface functionalization via TEC of Vim and Aam hc could be clearly confirmed by a significant increase in nitrogen (N1s) content, from 4.5 (OSTE) to 7.3 and 5.5 atom%, respectively. Vim is a reactive monomer and known to polymerize under radical condition, which could explain the relatively strong increase in nitrogen content using Vim.[47] Consequently, the high reactivity of Vim could have led to the formation of short polymer grafts on the surface, even at low concentrations and short reaction times.

In addition to XPS analysis, the impact of the different surface modifications was also investigated by water contact angle (WCA) measurements. The WCA of APFB reacted surface (62.4°) changed slightly compared to the reference surface (OSTE, 67.0°), which was assumed to be the result of the low reactivity, as already seen from the XPS data. A similar trend was observed for OSTE-ATFA, where the WCA was reduced more significantly to 41.1° upon modification. This was attributed to the polar nature of ATFA. As expected, increased hydrophobicity of the surface was achieved via functionalization with OFPB, which was confirmed by a WCA of 77.0°. Reduced WCAs of 35.0° (OSTE-AA), 25.1° (OSTE-AMA) and 55.2° (OSTE-AGE) were observed due to the introduction of hydroxyl, carboxylic acid and epoxide groups via surface TEC with AMA, AA and AGE. Similarly, WCAs of 38.5° (OSTE-Vim) and 55.4° (OSTE-Aam hc) validated the functionalization with Vim and Aam hc. This illustrates the versatility of the system providing successful surface

modification by TEC and that the surface properties of the microplate wells could be adjusted by the formation of a functional monolayer.

Additionally, thiol groups are known to serve as chain transfer agents in free radical polymerization reactions in order to reduce molecular weight of the polymers. Surface bound thiols can act in a similar way as reported earlier for other types of surfaces, where the surface could be grafted by termination of growing polymer chains.[48–50] In this study, we have expanded this SCT-FRP approach as an alternative method to TEC for controlled surface modification of OSTE materials. Different acrylic and methacrylic monomers containing polyethylene glycol (PEG) (via MPEGMA), a zwitterionic sulfobetaine (SBMA), fluorine (OFPA) and epoxide groups (GMA) were utilized. In this case, by running the photochemical reaction at a higher concentration, polymer grafting onto the well surfaces could be achieved by SCT-FRP in the presence of DMPA as radical photoinitiator, as shown in Scheme 1. Typically, the liquid monomers were used in a 1:2 volume ratio in ethanol, whereas SBMA, being a solid, was applied in a concentration of 2.4 M. In contrast to TEC, surface modification via SCT-FRP can be confirmed by IR spectroscopy, as illustrated in Figure 2.

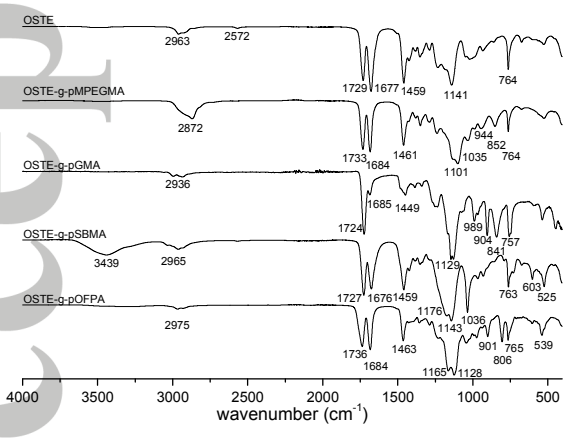

Figure 2 IR spectra of virgin OSTE surface and OSTE grafted via SCT FRP with various acrylate and methacrylate based polymer, such as MPEGMA, GMA, SBMA or OFPA

A clear indication of the formation of a thick surface layer by SCT-FRP is the full disappearance of the S-H stretch band at 2572 cm^{-1} upon surface polymerization of each monomer. The spectrum of OSTE-g-pMPEGMA showed a strong absorption at 1100 cm^{-1}, which can be assigned to C-O-C stretch vibration originating from the PEG side chain. An additional band at 904 cm^{-1} for the OSTE-g-pGMA is observed, which is the epoxide ring vibration. In the IR spectrum of the OSTE surface upon grafting with pSBMA, a band at 3439 cm^{-1} indicates the ammonium N-H stretch vibration. Furthermore a broadening of the C-O-C stretch absorption at 1143 cm^{-1} as well as the strong band at 1036 cm^{-1} confirms the presence of pSBMA. Surface grafting with pOFPA led to the appearance of carbon-fluorine bands at 1163, 806 and 539 cm^{-1}. XPS and WCA analysis corroborated these results, which are presented in Table 2.

Table 2. XPS data and static water contact angles (WCA) of virgin and grafted OSTE surfaces via SCT FRP with a variety of acrylate and methacrylate based polymers[a].

	C1s [atom%]	O1s [atom%]	N1s [atom%]	S2p [atom%]	F1s [atom%]	WCA [°]
OSTE	61.1 (60.6)	23.3±0.2 (24.9)	4.5±0.3 (4.1)	11.1±0.3 (10.4)		67.0±1.2
OSTE-g-pMPEGMA	65.6±0.6 (67.6)	30.1±0.2 (32.4)	0.5±0.4 (0.0)	3.9±0.2 (0.0)		25.4±3.6
OSTE-g-pGMA	70.7±0.4 (70.0)	28.7±0.4 (30.0)	0.5±0.1 (0.0)			69.6±7.5
OSTE-g-pSBMA	62.9±0.0 (61.1)	25.2±0.0 (27.8)	4.7±0.1 (5.6)	7.2±0.1 (5.6)		20.4±4.8
OSTE-g-pOFPA	43.2±0.6 (44.4)	11.1±0.3 (11.1)	0.5±0.1 (0.0)	1.3±0.3 (0.0)	44.0±1.3 (44.4)	118.1±1.9

[a] In parenthesis, theoretical atom composition of the virgin surface (OSTE) and monomers used for SCT FRP, results are based on three replicated measurements on the same surface (n=3)

XPS analysis of a pMPEGMA grafted surface (OSTE-g-pMPEGMA) showed significantly increased carbon and oxygen contents, which is consistent with the theoretical value of

MPEGMA. Combination with the simultaneous decrease in sulfur and nitrogen confirms the polymer grafting of the OSTE-g-pMPEGMA surface. Similar XPS results were achieved by polymer grafting with pGMA, where the oxygen and carbon content increased approaching the theoretical value of the monomer. The amount of nitrogen and sulfur was even lower compared to OSTE-g-pMPEGMA, indicating an even thicker pGMA layer. The theoretical atom composition of SBMA is more similar to that of the OSTE background, which leads to only minor changes in the atom composition as a result of grafting. However, the content of the individual atoms from the OSTE-g-pSBMA surface approximated the theoretical values of the SBMA monomer, substantiating the success of the grafting reaction. Compared to the aforementioned surface modification via TEC with OFPA, polymerization conditions (higher concentration, longer reaction time) lead here to the appearance of a much higher fluorine content of 44.0 atom% compared to the 7.1 atom% by TEC. Additionally, the total atom composition of the OSTE-g-pOFPA surface was found to be in good agreement with that of the pure monomer, which confirms the formation of a polymer layer on the surface under SCT-FRP conditions.

These presented changes in atom composition, upon polymer grafting with the individual monomers, were corroborated by the variation in WCAs of the reacted surfaces. Grafting with pMPEGMA increased the hydrophilic character, which was shown by a reduction in WCA from 67° (OSTE) to 25.4°. Similarly, a substantial hydrophilization was achieved by grafting with pSBMA (20.4°) confirming the surface reaction. The WCA increased slightly upon SCT-FRP using GMA (69.6°). OSTE-g-pOFPA exhibits a very high WCA of 118.1° and demonstrates the drastically increased hydrophobicity of the surface upon polymer grafting, which is significantly higher than the one obtained from TEC using the same monomer (77.0°). These results, together with the earlier discussed XPS and IR data, illustrate the potential for altering surface properties through selection of reaction conditions. Low

concentrations and short reaction times lead to addition of the acrylate to the thiol groups based on TEC. Increased concentrations and longer reaction times favor polymerization, which undergoes chain transfer or termination with surface thiols leading to a thicker surface coating. The application of either surface modification method, TEC or SCT-FRP, demonstrates the versatility of these grafting reactions in order to achieve high control over the surface functionality and properties.

The functionalized well bottom surfaces were subsequently used for enzyme immobilization. For this purpose, a rhodamine labelled horseradish peroxidase (Rho-HRP) dissolved in PBS buffer (pH7.3) was used as a model enzyme. Fluorescence intensity (FI) measurements were used to confirm the presence of immobilized enzyme on all surfaces. In order to evaluate qualitatively the amount of immobilized enzyme, FI measurements ($\lambda_{excitation}$ = 544 nm, $\lambda_{emission}$ = 595 nm) of the surfaces were conducted before (as reference) and after incubation with Rho-HRP. Figure 3 shows the reference corrected FI measurements of enzyme exposed TEC (A) and SCT-FRP modified surfaces (B).

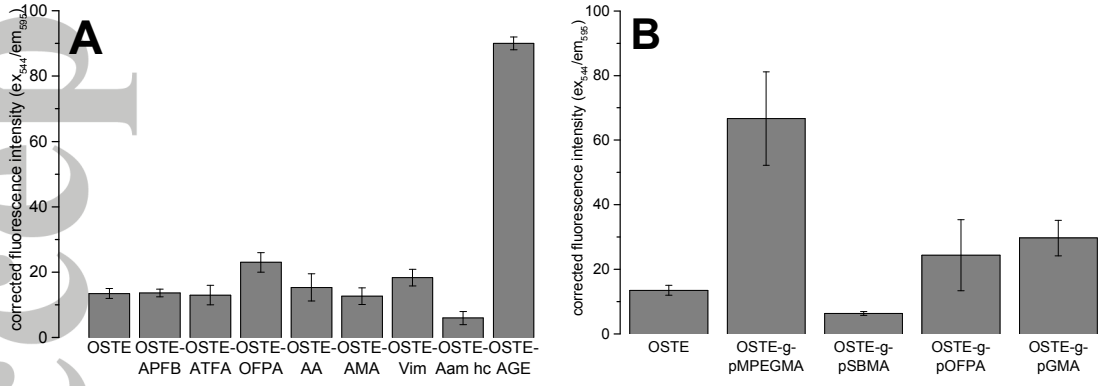

Figure 3. Reference corrected fluorescence intensity of virgin (OSTE) and functionalized surfaces via TEC (A) and SCT FRP (B) after immobilization of rhodamine labeled horseradish peroxidase (Rho-HRP), excitation at 544 nm and emission at 595 nm, standard deviations are based on three experimental replicates (n=3)

It can be seen that the native OSTE surface exhibited a substantial FI upon exposure to Rho-HRP (Figure 3A, OSTE), which relates to significant loading of labeled enzyme on the surface. TEC functionalized surfaces, such as APFB, ATFA, AA, AMA and Vim provided similar FI results and consequently comparable adsorption of Rho-HRP. Higher FI results are the consequence of OPFA modifications, which is an indication for increased enzyme loading. Accordingly the lower FI values of Aam hc compared to other functionalized surfaces suggest a lower enzyme coverage. Compared to all aforementioned surfaces, surface functionalization with epoxide groups due to the reaction with AGE leads to a drastic increase in FI upon exposure to enzyme, which is more than 6-fold higher compared to that of the native OSTE surface. Amine groups from lysine or thiols from cysteine residues within the enzyme structure are expected to react covalently with epoxide groups on the surface and thus create a higher enzyme loading.[51]

Similar measurements were performed with surfaces functionalized by SCT-FRP, as shown in Figure 3B. The highest FI was observed for pMPEGMA modified surfaces. This result was unexpected, since PEG surface grafts were reported in the literature to exhibit anti-fouling properties and therefore reduced unspecific protein adsorption.[52,53] In order to explain this discrepancy, FI of Rho-HRP was measured in solution in the presence of different MPEGMA concentrations, as presented in Figure S5. These results show a direct correlation of FI with increasing amounts of MPEGMA. This effect of FI enhancement for Rho-HRP in the presence of MPEGMA could indicate an artificially high loading of enzyme on the OSTE-g-pMPEGMA surfaces. Good biocompatibility and anti-fouling properties have also been described for zwitterionic polymers, such as pSBMA.[54–56] Herein, pSBMA grafted surfaces with an increased hydrophilicity, show a very low FI after enzyme immobilization, which reinforces the hypothesis of low enzyme loading on these surfaces. Surface functionalization by pOFPA under SCT-FRP conditions shows slightly increased FI compared to the native

OSTE surface, which is similar to that of TEC functionalized surface with OFPA (Figure 3A). Relatively similar enzyme loading based on comparable FI results were achieved by surface grafting with pGMA via SCT-FRP, even though the epoxide containing pGMA enables covalent immobilization.

A significant advantage of this platform is that biocatalytic activity of immobilized enzymes could be measured spectrophotometrically directly in a microplate reader by using a colorimetric assay. For immobilized Rho-HRP on the previously prepared surfaces by either TEC or SCT-FRP, 2,2′-azino-bis(3-ethylbenzothiazoline-6-sulfonic acid) diammonium salt (ABTS) was used as a colorimetric assay. The slope of absorbance, which correlated directly to the formed product, over time, was used to express the initial enzymatic activity of the particular surfaces, as shown in Figure 4A for TEC modified surfaces.

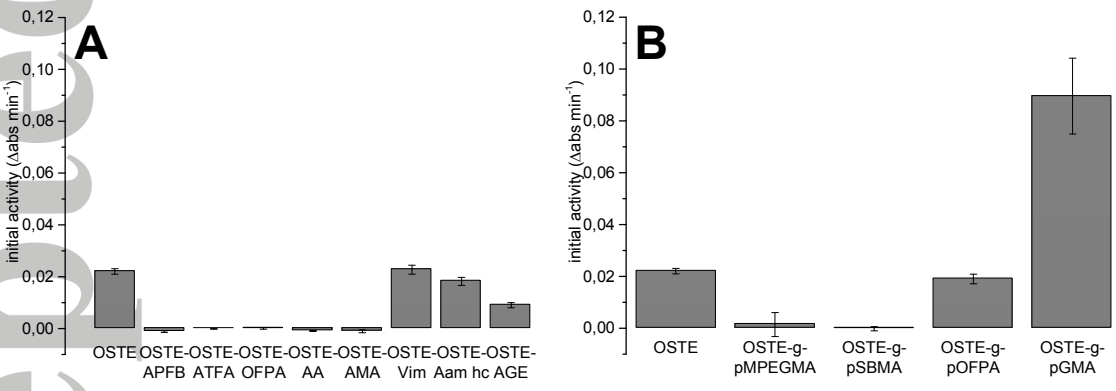

Figure 4. Initial enzyme activity of Rho-HRP immobilized on virgin (OSTE) and functionalized surfaces via TEC (A) with various ene compounds and SCT FRP (B) with various acrylate and methacrylate based polymers, standard deviations are based on three experimental replicates (n=3)

From these results, a clear difference in Rho-HRP activity from the individual surface modification, upon enzyme immobilization, can be seen. In general, the displayed activities are caused by two factors, enzyme loading and biocatalytic activity, which both directly

affected the overall activity. This directly reflects the influence of the individual surface chemistry. The native OSTE surface exhibited an activity of 0.022 Δabs min^{-1}. Even though TEC modified surfaces with fluorinated (APFB, ATFA and OFPA), hydroxyl (AA) and carboxylic acid containing compounds (AMA) expressed a substantial enzyme loading, these were not active at all (see Figure 4A), which suggested an unfavorable environment for the enzyme by these functional groups. On the contrary, imidazole (Vim) and amine (Aam hc) functional surfaces showed the highest initial activities for TEC modified surfaces of about 0.023 and 0.018 Δabs min^{-1}, respectively. These results indicate that amine, imidazole as well as thiol groups from the native OSTE surface provide a more beneficial local environment towards the enzyme and thus, activity was retained. FI indicated high enzyme coverage on surfaces, functionalized with epoxide groups (OSTE-AGE). However, the resulting initial activity was only 0.009 Δabs min^{-1}, which is significantly lower than that of OSTE, Vim and Aam hc surfaces. It was assumed that this is a result of unfavorable interaction of the surface with the enzyme, which is known to have a significant impact during the adsorption-covalent immobilization mechanism onto epoxy supports.[6] As a consequence, blocking of the active site or conformational changes of the enzyme could have resulted in the low activity.

Likewise, the initial enzyme activity was determined from surfaces grafted with polymer layers by SCT-FRP after Rho-HRP immobilization (see Figure 4B). Hydrophilic surfaces due to grafting with pMPEGMA and pSBMA tend to be enzymatically inactive. The low activity of OSTE-g- pSBMA correlates directly with the low enzyme loading, which was determined by FI measurements. The low activity of pMPEGMA grafted OSTE surfaces relates well with the anti-fouling nature of PEG grafted surfaces. Their tendency to FI enhancement indicates an artificially high enzyme loading. Surfaces which were grafted with hydrophobic pOFPA by SCT-FRP, exhibit a similar activity (0.019 Δabs min^{-1}) compared to the original OSTE surface, which correlates well with the results from the FI measurements. The activity was

found to be substantially higher than those of surfaces with OFPA monolayer functionalization via TEC, even though both surfaces show comparable enzyme loadings. Thus, increased hydrophobic interactions between the enzyme and the surface created by a thicker surface layer seems to have a positive effect on the enzyme activity A high HRP activity (0.07 Δabs min^{-1}) can be seen from OSTE-g-pGMA surfaces prepared by SCT-FRP. GMA based polymers, bearing epoxide groups, allow covalent attachment of HRP and has already been used in various studies for enzyme immobilization.[57,58] Compared to the epoxide functional monolayer formed from AGE by TEC, the pGMA surface layer shows a decreased enzyme loading, but substantial improvement of enzymatic activity.

4. Conclusions

A single, versatile platform for testing a broad variety of surface chemistries as candidates for supports for enzyme immobilization is proposed in this study, with the main objective of making identification of suitable surface/enzyme combinations in a more facile and time saving manner. This strategy indeed permits a faster, easier and broader surface–enzyme screening compared to the traditional "trial and error" method generally involving resins. The results showed that the STE/OSTE microplate is suitable for colorimetric measurements above 340 nm and the thiol functional wells can be functionalized through either TEC or SCT-FRP providing a broad selection of functional surfaces. We have shown how TEC/SCT-FRP can be exploited to prepare functional monolayers (TEC) or thicker polymer layers (SCT-FRP). Thus, different surface functionalities, such as hydroxyl, carboxylic acid, amine, fluorine, imidazole, epoxide, PEG and zwitterionic groups could be introduced, which was confirmed by XPS analysis. Through immobilization of HRP as a model enzyme, the effects of surface/enzyme interactions were illustrated in the microplate, showing clear correlations between surface functionalities and enzymatic activities. HRP displayed improved activities when attached directly to imidazole, thiol and amine functional surfaces, compared to hydroxyl, fluorinated, carboxylic acid or epoxide containing surfaces. Immobilization of HRP on pOFPA modified surfaces demonstrated a significant activity, which might be caused by increased hydrophobic interactions between enzyme and surface. Based on the initial biocatalytic activities relative to the surface chemistry it is possible to identify candidates that should be tested in depth for enzyme immobilization. Thereby we have demonstrated the potential of this screening platform to be used for other enzymes, facilitating the identification of suitable surfaces for immobilization. Furthermore, by use of such a platform it would be possible to determine the influence of other parameters, such as temperature, pH, and e.g. substrate concentration.

Supporting Information

Supporting Information is available from the Wiley Online Library or from the author.

Acknowledgements

The authors wish to thank the Aage and Johanne Louis-Hansens Endowment for financial support.

References

1. DiCosimo R, McAuliffe J, Poulose AJ, Bohlmann G. Industrial use of immobilized enzymes. *Chem Soc Rev*. 2013;42(15):6437-74.
2. Cantone S, Ferrario V, Corici L, Ebert C, Fattor D, Spizzo P, Gardossi L. Efficient immobilisation of industrial biocatalysts: criteria and constraints for the selection of organic polymeric carriers and immobilisation methods. *Chem Soc Rev*. 2013;42(15):6262-76.
3. Mateo C, Palomo JM, Fernandez-Lorente G, Guisan JM, Fernandez-Lafuente R. Improvement of enzyme activity, stability and selectivity via immobilization techniques. *Enzyme Microb Technol*. 2007;40(6):1451-1463.
4. Minteer SD. *Enzyme Stabilization and Immobilization*. Vol 1504. 2nd ed. (Minteer SD, ed.). Springer Science+Business Media; 2010.
5. Balcão VM, Vila MMDC. Structural and functional stabilization of protein entities: State-of-the-art. *Adv Drug Deliv Rev*. 2015;93:25-41.
6. Mateo C, Grazú V, Pessela BCC, Montes T, Palomo JM, Torres R, López-Gallego F, Fernàndez-Lafuente R, Guisán JM. Advances in the design of new epoxy supports for enzyme immobilization–stabilization. *Biochem Soc Trans*. 2007;35(6):1593-1601.
7. Kallenberg AI, van Rantwijk F, Sheldon RA. Immobilization of Penicillin G Acylase: The Key to Optimum Performance. *Adv Synth Catal*. 2005;347(7-8):905-926.
8. Sheldon RA, van Pelt S. Enzyme immobilisation in biocatalysis: why, what and how.

Chem Soc Rev. 2013;42(15):6223-35.

9. Mateo C, Palomo JM, van Langen LM, van Rantwijk F, Sheldon RA. A new, mild cross-linking methodology to prepare cross-linked enzyme aggregates. *Biotechnol Bioeng*. 2004;86(3):273-6.
10. Mohamad NR, Marzuki NHC, Buang NA, Huyop F, Wahab RA. An overview of technologies for immobilization of enzymes and surface analysis techniques for immobilized enzymes. *Biotechnol Biotechnol Equip*. 2015;29(2):205-220.
11. Ying L, Kang ET, Neoh KG. Covalent immobilization of glucose oxidase on microporous membranes prepared from poly(vinylidene fluoride) with grafted poly(acrylic acid) side chains. *J Memb Sci*. 2002;208(1-2):361-374.
12. Secundo F. Conformational changes of enzymes upon immobilisation. *Chem Soc Rev*. 2013;42(15):6250-61.
13. Rodrigues RC, Ortiz C, Berenguer-Murcia Á, Torres R, Fernández-Lafuente R. Modifying enzyme activity and selectivity by immobilization. *Chem Soc Rev*. 2013;42(15):6290-307.
14. Talbert JN, Goddard JM. Enzymes on material surfaces. *Colloids Surfaces B Biointerfaces*. 2012;93:8-19.
15. Santos JCS Dos, Barbosa O, Ortiz C, Berenguer-Murcia A, Rodrigues RC, Fernandez-Lafuente R. Importance of the Support Properties for Immobilization or Purification of Enzymes. *ChemCatChem*. 2015;7(16):2413-2432.
16. Hamlin RE, Daytong TL, Johnson LE, Johal MS. A QCM study of the immobilization of b-galactosidase on polyelectrolyte surfaces: Effect of the terminal polyion on enzymatic surface activity. *Langmuir*. 2007;23(8):4432-4437.
17. Malinin AS, Rakhnyanskaya AA, Bacheva A V, Yaroslavov AA. Activity of an Enzyme Immobilized on Polyelectrolyte Multilayers. *Polym Sci Ser A*. 2011;53(1):52-56.

18. Cheng Z, Teoh S-H. Surface modification of ultra thin poly (ε-caprolactone) films using acrylic acid and collagen. *Biomaterials*. 2004;25(11):1991-2001.

19. Misson M, Dai S, Jin B, Chen BH, Zhang H. Manipulation of nanofiber-based β-galactosidase nanoenvironment for enhancement of galacto-oligosaccharide production. *J Biotechnol*. 2016;222:56-64.

20. Cao L. Covalent Enzyme Immobilization. In: *Carrier-Bound Immobilized Enzymes: Principles, Application and Design*. WILEY-VCH; 2006:169-316.

21. Huang J, Li X, Zheng Y, Zhang Y, Zhao R, Gao X, Yan H. Immobilization of Penicillin G Acylase on Poly[(glycidyl methacrylate)-co-(glycerol monomethacrylate)]-Grafted Magnetic Microspheres. *Macromol Biosci*. 2008;8(6):508-515.

22. Bayramoglu G, Karagoz B, Altintas B, Arica MY, Bicak N. Poly(styrene–divinylbenzene) beads surface functionalized with di-block polymer grafting and multi-modal ligand attachment: performance of reversibly immobilized lipase in ester synthesis. *Bioprocess Biosyst Eng*. 2011;34(6):735-46.

23. Chen H, Teramura Y, Iwata H. Co-immobilization of urokinase and thrombomodulin on islet surfaces by poly(ethylene glycol)-conjugated phospholipid. *J Control Release*. 2011;150(2):229-234.

24. Manta C, Ferraz N, Betancor L, Antunes G, Batista-Viera F, Carlsson J, Caldwell K. Polyethylene glycol as a spacer for solid-phase enzyme immobilization. *Enzyme Microb Technol*. 2003;33(7):890-898.

25. Mahoney KW, Talbert JN, Goddard JM. Effect of polyethylene glycol tether size and chemistry on the attachment of lactase to polyethylene films. *J Appl Polym Sci*. 2013;127(2):1203-1210.

26. Goddard JM, Hotchkiss JH. Polymer surface modification for the attachment of bioactive compounds. *Prog Polym Sci*. 2007;32(7):698-725.

27. Campos LM, Meinel I, Guino RG, Schierhorn M, Gupta N, Stucky GD, Hawker CJ. Highly Versatile and Robust Materials for Soft Imprint Lithography Based on Thiol-ene Click Chemistry. *Adv Mater*. 2008;20(19):3728-3733.

28. Khire VS, Yi Y, Clark NA, Bowman CN. Formation and surface modification of nanopatterned thiol-ene substrates using step and flash imprint lithography. *Adv Mater*. 2008;20:3308-3313.

29. Carlborg CF, Haraldsson T, Öberg K, Malkoch M, van der Wijngaart W. Beyond PDMS: off-stoichiometry thiol–ene (OSTE) based soft lithography for rapid prototyping of microfluidic devices. *Lab Chip*. 2011;11(18):3136.

30. Mongkhontreerat S, Öberg K, Erixon L, Löwenhielm P, Hult A, Malkoch M. UV initiated thiol–ene chemistry: a facile and modular synthetic methodology for the construction of functional 3D networks with tunable properties. *J Mater Chem A*. 2013;1(44):13732-13737.

31. Lowe AB. Thiol-ene "click" reactions and recent applications in polymer and materials synthesis. *Polym Chem*. 2010;1(1):17-36.

32. Tähkä SM, Bonabi A, Nordberg ME, Kanerva M, Jokinen VP, Sikanen TM. Thiol-ene microfluidic devices for microchip electrophoresis: Effects of curing conditions and monomer composition on surface properties. *J Chromatogr A*. 2015;1426:233-240.

33. Mazurek P, Daugaard AE, Skolimowski M, Hvilsted S, Skov AL. Preparing mono-dispersed liquid core PDMS microcapsules from thiol–ene–epoxy-tailored flow-focusing microfluidic devices. *RSC Adv*. 2015;5(20):15379-15386.

34. Durham OZ, Norton HR, Shipp DA. Functional polymer particles via thiol–ene and thiol–yne suspension "click" polymerization. *RSC Adv*. 2015;5(82):66757-66766.

35. Aimetti AA, Machen AJ, Anseth KS. Poly(ethylene glycol) hydrogels formed by thiol-ene photopolymerization for enzyme-responsive protein delivery. *Biomaterials*. 2009;30(30):6048-54.

36. Lovelady E, Kimmins SD, Wu J, Cameron NR. Preparation of emulsion-templated porous polymers using thiol–ene and thiol–yne chemistry. *Polym Chem*. 2011;2(3):559-562.

37. Zhang J, Chen Y, Brook MA. Facile Functionalization of PDMS Elastomer Surfaces Using Thiol− Ene Click Chemistry. *Langmuir*. 2013;29(40):12432-12442.

38. Wasserberg D, Steentjes T, Stopel MHW, Huskens J, Blum C, Subramaniam V, Jonkheijm P. Patterning perylenes on surfaces using thiol–ene chemistry. *J Mater Chem*. 2012;22:16606-16610.

39. Han X, Wu C, Sun S. Photochemical reactions of thiol-terminated self-assembled monolayers (SAMs) for micropatterning of gold nanoparticles and controlled surface functionality. *Appl Surf Sci*. 2012;258(12):5153-5156.

40. Tan KY, Ramstedt M, Colak B, Huck WTS, Gautrot JE. Study of thiol–ene chemistry on polymer brushes and application to surface patterning and protein adsorption. *Polym Chem*. 2016;7(4):979-990.

41. Pardon G, Saharil F, Karlsson JM, Supekar O, Carlborg CF, van der Wijngaart W, Haraldsson T. Rapid mold-free manufacturing of microfluidic devices with robust and spatially directed surface modifications. *Microfluid Nanofluidics*. 2014;17(4):773-779.

42. Carlborg CF, Moraga F, Saharil F, van der Wijngaart W, Haraldsson T. Rapid Permanent Hydrophilic and Hydrophobic Patterning of Polymer Surfaces Via Off-Stoichiometry Thiol-Ene (OSTE) Phtografting. In: *Proceedings Micro Total Analysis Systems*. ; 2012:677-679.

43. Feidenhans'l NA, Lafleur JP, Jensen TG, Kutter JP. Surface functionalized thiol-ene waveguides for fluorescence biosensing in microfluidic devices. *Electrophoresis*. 2014;35(2-3):282-288.

44. Cakmakci E, Danis O, Demir S, Mulazim Y, Kahraman MV. Alpha-amylase immobilization on epoxy containing thiol-ene photocurable materials. *J Microbiol*

Biotechnol. 2013;23:205-210.

45. Childs BRE, Bardsley WG. The Steady-State Kinetics of Peroxidase with 2,2'-Azino-di-(3-ethylbenzthiazoline- 6-sulphonic acid) as Chromogen. *Biochem J*. 1975;145:93-103.

46. Hansson S, Antoni P, Bergenudd H, Malmström E. Selective cleavage of polymer grafts from solid surfaces: assessment of initiator content and polymer characteristics. *Polym Chem*. 2011;2(3):556-558.

47. Fodor C, Bozi J, Blazsó M, Iván B. Thermal behavior, stability, and decomposition mechanism of poly(N-vinylimidazole). *Macromolecules*. 2012;45(22):8953-8960.

48. Liu S, Zhou F, Di D, Jiang S. Surface-confined radical chain transfer. *Colloids Surfaces A Physicochem Eng Asp*. 2004;244(1-3):87-93.

49. Wang S, Zhou Y, Guan W, Ding B. One-step copolymerization modified magnetic nanoparticles via surface chain transfer free radical polymerization. *Appl Surf Sci*. 2008;254(16):5170-5174.

50. Bertin A, Schlaad H. Mild and versatile (Bio-)functionalization of glass surfaces via thiol-ene photochemistry. *Chem Mater*. 2009;21(24):5698-5700.

51. Jiang H, Xu F-J. Biomolecule-functionalized polymer brushes. *Chem Soc Rev*. 2013;42(8):3394-426.

52. Xu FJ, Neoh KG, Kang ET. Bioactive surfaces and biomaterials via atom transfer radical polymerization. *Prog Polym Sci*. 2009;34(8):719-761.

53. Xiu KM, Cai Q, Li JS, Yang XP, Yang WT, Xu FJ. Anti-fouling surfaces by combined molecular self-assembly and surface-initiated ATRP for micropatterning active proteins. *Colloids Surf B Biointerfaces*. 2012;90:177-83.

54. Fristrup CJ, Jankova K, Hvilsted S. Surface-initiated atom transfer radical polymerization—a technique to develop biofunctional coatings. *Soft Matter*. 2009;5(23):4623.

55. Yue W-W, Li H-J, Xiang T, Qin H, Sun S-D, Zhao C-S. Grafting of zwitterion from polysulfone membrane via surface-initiated ATRP with enhanced antifouling property and biocompatibility. *J Memb Sci*. 2013;446:79-91.

56. Xiang T, Zhang L-S, Wang R, Xia Y, Su B-H, Zhao C-S. Blood compatibility comparison for polysulfone membranes modified by grafting block and random zwitterionic copolymers via surface-initiated ATRP. *J Colloid Interface Sci*. 2014;432:47-56.

57. Xu FJ, Cai QJ, Li YL, Kang ET, Neoh KG. Covalent immobilization of glucose oxidase on well-defined poly(glycidyl methacrylate)-Si(111) hybrids from surface-initiated atom-transfer radical polymerization. *Biomacromolecules*. 2005;6(2):1012-20.

58. Shen Y, Guo W, Qi L, Qiao J, Wang F, Mao L. Immobilization of trypsin via reactive polymer grafting from magnetic nanoparticles for microwave-assisted digestion. *J Mater Chem B*. 2013;1(17):2260-2267.